

A Fully Localised Periodic Orbit In Plane Poiseuille Flow

STEFAN ZAMMERT¹ † AND BRUNO ECKHARDT^{1,2}

¹ Fachbereich Physik, Philipps-Universität Marburg, Renthof 6, D-35032 Marburg, Germany

² J.M. Burgerscentrum, Delft University of Technology, Mekelweg 2, 2628 CD Delft, The Netherlands

(Received 3 December 2024)

We present a fully localised exact coherent structure of the Navier-Stokes equation for plane Poiseuille flow in the form of a relative periodic orbit. The structure is obtained from extended ones in smaller, periodically continued domains, by increasing the length to obtain downstream localisation and then by increasing the width to achieve spanwise localisation. The structure consists of a uniformly propagating envelope and spanwise modulations that move with a different phase speed, hence causing the periodic modulations. The upstream side of the state varies little with Reynolds number, but the length of the downstream tail increases with Re .

1. Introduction

The study of coherent structures in small domains, often referred to as 'minimal flow units', has provided considerable insight into the phase space structure and the transition dynamics of shear flows without linear instabilities, such as pipe flow or plane Couette flow and various boundary layers (e.g. Kreilos & Eckhardt (2012) and references therein). For an understanding of the fascinating spatio-temporal dynamics in the transition region, where intriguing patterns of alternating laminar and turbulent dynamics (Barkley & Tuckerman 2005; Duguet *et al.* 2010) and a complicated evolution that is connected to directed percolation (Moxey & Barkley 2010; Avila *et al.* 2011) can be observed. The interest in localised solutions arises also from the possibility to use them as building blocks for the more complicated spatial patterns, such as the turbulent spots observed in plane Couette or plane Poiseuille flow in various experimental (e.g. Carlson *et al.* 1982; Dauchot & Daviaud 1995; Hegseth 1996; Lemoult *et al.* 2013a) and numerical (e.g. Henningson *et al.* 1987; Lundbladh & Johansson 1991; Schumacher & Eckhardt 2001) studies.

The spatially extended exact coherent structures (Wang *et al.* 2007; Gibson *et al.* 2009) in the form of stationary states without any time-dependence, travelling waves where a pattern moves downstream with a fixed speed, or relative periodic orbits that return to the initial pattern except for a displacement. Examples of spanwise localized states have been identified by Schneider *et al.* (2010a,b), Gibson & Brand (2014) and Zammert & Eckhardt (2014) for plane Couette and plane Poiseuille flow. Streamwise localised exact solutions were found for the case of 2D plane Poiseuille flow by Price *et al.* (1993) and for pipe flow by Avila *et al.* (2013) and Chantry *et al.* (2013). Spanwise localized states in plane Poiseuille flow show a complicated temporal dynamics (Zammert & Eckhardt 2014) that has also been seen in the asymptotic suction boundary layer Khapko *et al.* (2013a,b).

† Email address for correspondence: stefan.zammert@physik.uni-marburg.de

In this paper we present a fully localised coherent structure for plane Poiseuille flow. We identify it using the method of edge tracking Skufca *et al.* (2006) in small domains, and show that it becomes localised in the streamwise and spanwise direction when the computational domain is enlarged. We trace out the bifurcations and stability properties of this state between its point of appearance near $Re = 1083$ to about $Re = 3500$.

2. The edge state in short domains - A traveling wave

We study the incompressible plane Poiseuille flow (PPF), the pressure driven flow between two infinitely extended parallel plates. With the x -axis along the flow direction, the plates are parallel to the x - z plane at $y = \pm h$. The Reynolds number is based on h , the centre-line velocity U_0 and the kinematic viscosity ν , so that $Re = U_0 d / \nu$ and the laminar profile becomes $U(y) = (1 - y^2)$. In all our simulations constant mass-flux is imposed. The velocity fields used in the remaining paper are the deviations from the laminar profile, denoted $\mathbf{u} = (u, v, w)$, where u , v , and w are the streamwise, wallnormal and spanwise velocity components, respectively.

The numerical simulations are based on the spectral code *channelflow*, developed and maintained by Gibson (2012). The package provides a Newtons-method (Viswanath 2007) for searching exact solutions as well as tools for continuation and stability analysis. For the linear algebra routines used in the Newtons-method and the eigenvalues calculation the *Eigen* package (Guennebaud, Jacon & Others 2010) is used. The method of edge tracking algorithm is described, e.g., by Toh & Itano (2003), Skufca *et al.* (2006), Schneider *et al.* (2008) and Dijkstra *et al.* (2014).

We started off with edge tracking starting from a random initial condition in a periodically continued small domain with streamwise length L_x of 2π and spanwise width L_z of 2π with a numerical resolution of $N_x \times N_y \times N_z = 32 \times 65 \times 48$ and a Reynolds number of 1400. For this Re plane Poiseuille flow shows persistent turbulence although it is far below the critical Reynolds number of 5772 (Orszag 1971). Edge tracking usually converges quickly to one travelling wave, referred to as TW_E in the following. This state has two symmetries, a mirror symmetry with respect to the mid-plane, and a shift and reflect symmetry in the spanwise direction,

$$s_y : [u, v, w](x, y, z) = [u, -v, w](x, -y, z), \quad (2.1)$$

$$s_z \tau_x : [u, v, w](x, y, z) = [u, v, -w](x + L_x/2, y, -z). \quad (2.2)$$

The state is dominated by a strong low speed streak in the midplane and pairs of vortices at the top and bottom plate and extends in all three directions. It is qualitatively different from the travelling waves in PPF described by Waleffe (1998, 2003) and Nagata & Deguchi (2013), but it has the same symmetry as TW1-1 from Gibson & Brand (2014).

Stability analysis of the travelling wave shows that it has one unstable eigenvalue for $510 < Re < 5850$ so that its stable manifold is of co-dimension one so that the transition scenario is similar to the one described in Kreilos & Eckhardt (2012). A stability analysis of the continued periodic state in a longer domain shows that already for $L_x = 4\pi$ the state has an additional pair of complex conjugated eigenvalues for $Re < 1785$. Further doubling of the domain size adds more unstable directions, so that, e.g., for $L_x = 8\pi$ and $Re = 1400$ the wave has 5 unstable eigenvalues. The larger domains allow for long-wavelength instabilities that are precursors to localisation (Melnikov *et al.* 2014; Chantry *et al.* 2013).

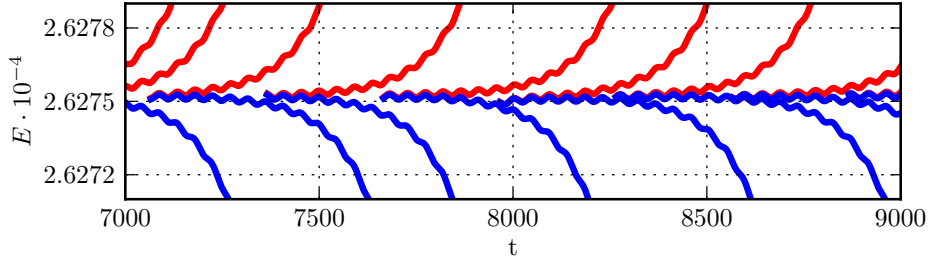


FIGURE 1. Edge tracking in a computational domain of length $L_x = 32\pi$ and width $L_z = 2\pi$. Shown are the energies of trajectories that turn turbulent (red) and laminar (blue), respectively. The edge state bracketed by these trajectories oscillates periodically in energy.

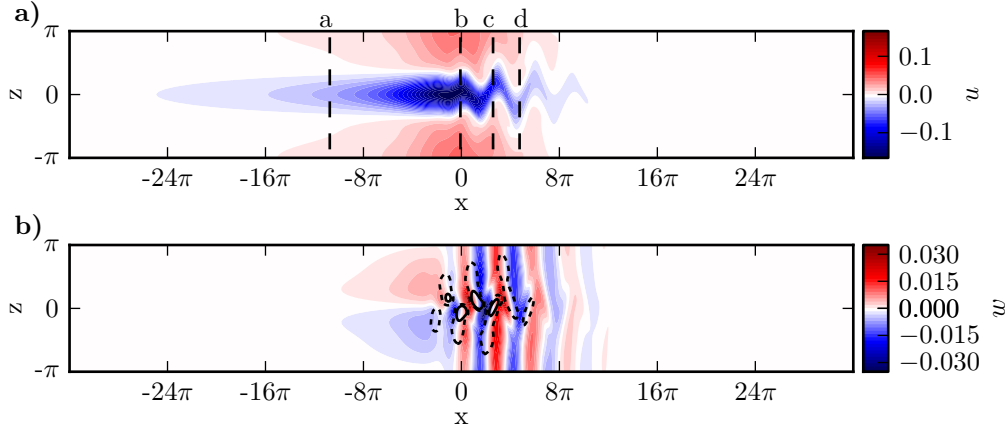


FIGURE 2. Velocities in the mid-plane for the edge state PO_E at $Re=1410$. Shown are the (a) streamwise velocity and (b) downstream velocities. The black lines in (a) mark the positions of the spanwise wall-normal cross sections in 3 (a)-(d). The solid and dashed lines in (b) are iso-contours of the Q-vortex criterion (Jeong & Hussain (1995)) at levels of 0.001 and 0.0001, respectively. The direction of the flow is from left to right.

3. Streamwise localised periodic orbits in long domains

In a longer domain of length 32π but the same width 2π and Reynolds number $Re = 1400$, edge tracking converged to a state that at first glance looks like a state of constant energy, $E(\mathbf{u}) = (\int \mathbf{u}^2 dx dy dz)/(2V)$. However, closer inspection of the timetrace in figure 1 reveals that it is not constant but shows a regular oscillation with an amplitude of order 10^{-8} . This oscillation is not a numerical artefact but reflects properties of the edge state, as we now show.

Although the initial velocity field fills the entire domain, the flow state obtained by edge tracking is localised in streamwise direction. Using this state as an initial condition in a Newton search, we quickly converged to a streamwise localised relative periodic orbit. For further study we transferred the state to a computational domain of length 64π , which is possible because of its streamwise localisation. We use a resolution of $768 \times 65 \times 48$ and check our results with a higher spanwise resolution of $N_z = 80$. The streamwise and the spanwise velocity components in the mid-plane are shown in figure 2. Cross-sections for $Re=1400$ for different streamwise positions are shown in figure 3 (a) - (d) and streamwise averaged velocity is shown in (e). These visualisations show that the orbit has a mirror symmetry and is dominated by a strong narrow low speed streak and a weak and extended high speed streak. It is therefore very similar to the travelling

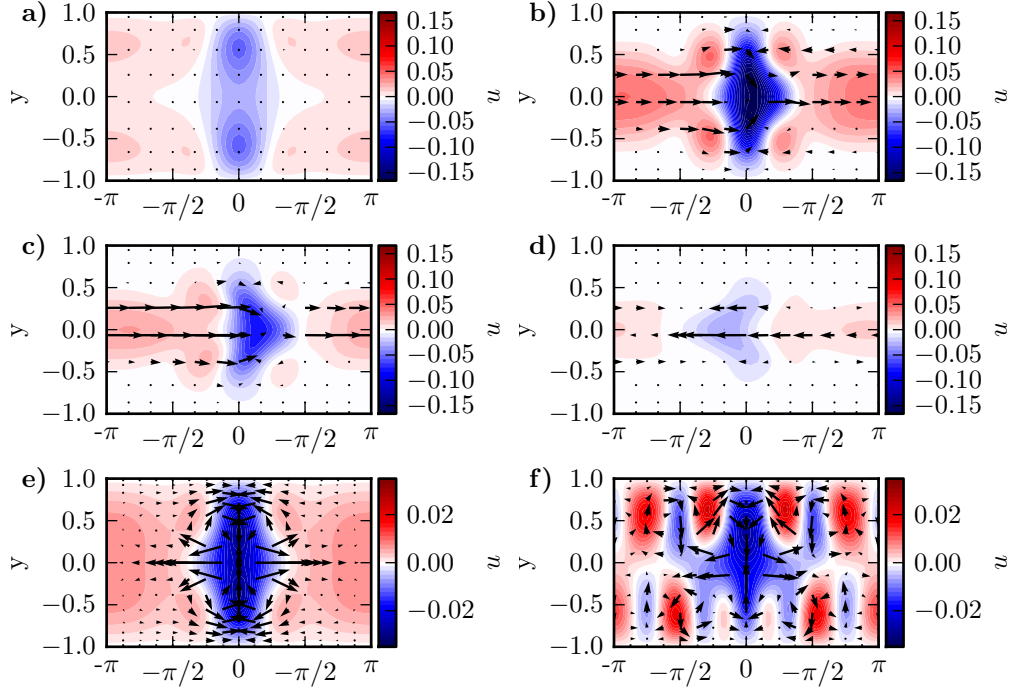


FIGURE 3. (a) - (d) Cross sections of the edge state PO_E at $Re = 1400$ at the downstream positions indicated in figure 2(b). The in-plane components of the velocity are indicated by arrows and the streamwise component is colour coded. (e) and (f) show the streamwise-averages of PO_E at $Re = 1410$ and of the orbit that bifurcates from it, PO_{asy} , at $Re = 1625$, respectively.

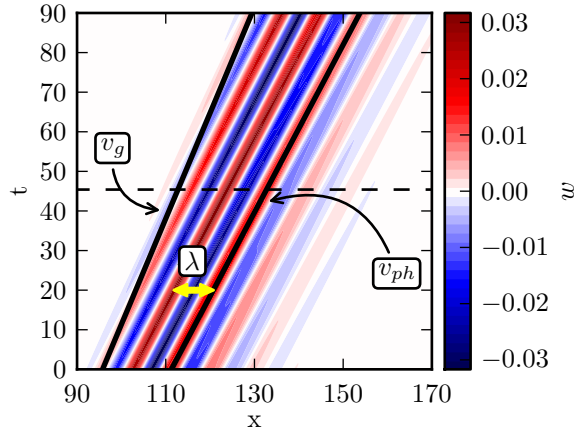


FIGURE 4. Space-time-display of the spanwise velocity of the periodic orbit PO_E in the mid-plane $y = 0$ at $z = 0$ for $Re=1400$. The solid black lines indicate the group velocity v_g and the phase velocity v_{ph} for one of the maxima. The wavelength λ of the internal modulations varies along the state. The dashed black lines marks one period in energy, which is only half a period of the state.

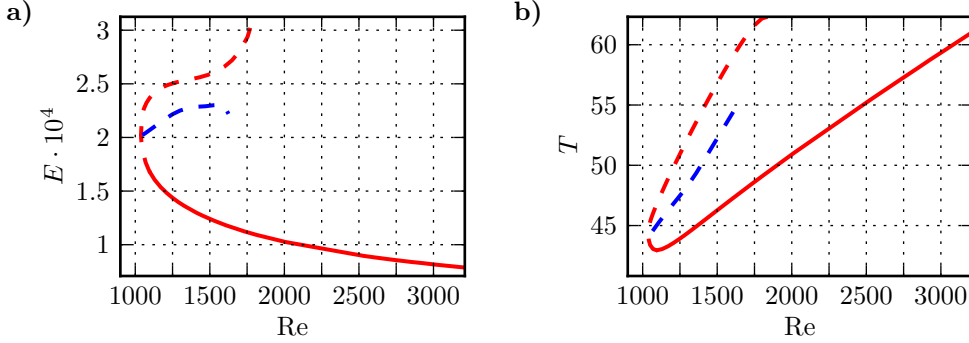


FIGURE 5. Bifurcation diagram for the coherent structures. (a) minimum energy of the localised periodic orbit (red) and the asymmetric orbit (blue) vs Re . In both cases the minimum in energy over the period is shown. The stability of the orbit is indicated by the linetype, solid for a single unstable direction, and dashed for more than one. (b) Variation of the periods in energy vs. Re .

wave TW_E . In particular, a visualisation of the streamwise averaged flow for TW_E is qualitatively identical to figure 3 (e).

The complex spatial propagation pattern of the wave can be seen in plots of the spanwise velocity in the midplane at $z = 0$ vs. time, figure 4. After two periods in energy, the state returns except for a downstream shift. After one period in energy it returns up to a symmetry operation $s_z : [u, v, w](x, y, z) = [u, v, -w](x, y, -z)$ and a shift that is half the one after two periods. The figure clearly shows a group velocity v_g for the envelope of the state, and a phase velocity v_{ph} for the underlying structures. The group velocity v_g can be read off from the period in energy, as distance travelled over two periods divided by the two periods. The corresponding line in the figure shows that this follows the envelope rather well. The structures underneath the envelope move with a different velocity, that can be read off from the slope of the maxima. However, the wavelength λ of the spanwise modulations varies slightly with position and is slightly larger at the front than in the centre and towards the end of the state. Therefore, also the velocity of each maximum varies slightly, so that the phase velocity depends on the position within the state.

Using a continuation method (see e.g. Dijkstra *et al.* 2014) it is easily possible to track the state in Re . It turns out that the periodic orbit exists down to $Re \approx 1038$, where it is created in a saddle node bifurcation. Furthermore, it is also possible to identify the upper branch of the periodic orbit. Bifurcation diagrams using the minimum of the energy and the period of the orbit are shown in figure 5.

A stability analysis of the state shows that for $Re > 1100$ the lower branch has one unstable direction. Therefore, for these Reynolds numbers the state is an edge state whose stable manifold can separate the state space into two parts. For other values of Re the periodic orbit has more than one unstable direction. The bifurcation at $Re = 1100$ is a Sacker-Neimark bifurcation that breaks the s_y symmetry. This bifurcation is followed by further bifurcations resulting in eight unstable directions for the lower branch. One of the bifurcations of the lower branch is a pitchfork bifurcation that breaks the s_y symmetry and creates an asymmetric periodic orbit (PO_{asy}). The image of the state in figure 3 (f) shows that it is more complex than PO_E and is more similar to a turbulent state. The bifurcations and the properties of the states are summarised in figure 5.

For a further investigation of the periodic orbit we study the total energy density of

the deviation from the laminar flow as a function of the streamwise position

$$E_{\perp}(x) = \frac{1}{2L_z} \int_0^{L_z} \int_{-1}^1 \mathbf{u}^2 dydz \quad (3.1)$$

and the density of the cross flow energy

$$E_{\perp,c}(x) = \frac{1}{2L_z} \int_0^{L_z} \int_{-1}^1 v^2 + w^2 dydz. \quad (3.2)$$

The energy densities for the periodic orbit at $Re = 2010$ (at the time of minimum energy) are shown in figure 6(a). One can identify a small area with relatively high cross flow energy at the front of the state. In this region the cross flow motion draws energy from the laminar profile and transfers it into streamwise velocity, which then drives streaks and causes a steep increase of the total energy density at the front of the state. The energy in the streamwise velocity has its maximum at a downstream position where the cross-flow energy is already very low again. In the absence of cross flow motion the streaks decay viscously, which results in the long downstream tail of the state.

Based on the energy density one can introduce two characteristic length scales for PO_E , defined as the distances from the maximum of the energy density to the points upstream (l_u) and downstream (l_d) where the energy has dropped to half the maximum value. These length scales vs. Re are shown in figure 6(b). On the upstream side, the energy drops off quickly, on a length scale that varies very little with Re . On the downstream side, the energy drops off more slowly, on a length scale that increases linearly with Re . The origin of this scaling is the viscous decay of the streaks on a time scale proportional to Re , which then is translated into a spatial scale proportional to Re by the essentially constant advection velocity.

Although the structure becomes longer with increasing Re , for the lower branch the total energy and also the maximum of the energy density decrease with increasing Re (see figure 5). In finite domains the increasing length of the structures will cause interferences between head and tail and a loss of localisation. For instance, continuation of PO_E to high Re in a box of length 32π shows that the orbit connects to the streamwise extended travelling wave TW_E at $Re \approx 5385$ with a wavelength of 2.66π . This is documented in figure 7 in a plot of the energy densities vs. Re . For low Re there is a pronounced maximum in the densities, but for increasing Re the differences decrease and finally at $Re \approx 5380$ the uniform energy density corresponding to the travelling wave is obtained. Turned the other way round, the localised state arises out of a streamwise long-wavelength instability of a travelling wave, very much as the long wavelength instabilities discussed in plane Couette flow (Melnikov *et al.* 2014) or in pipe flow (Chantry *et al.* 2013).

4. A fully localised periodic orbit

The periodic orbits found in the domain with $L_z = 2\pi$ are localised in the streamwise direction and also show early signs of localisation in the spanwise direction. Because, close to the strong low speed streak the energy density is much higher than in the area of the weak high speed streak. To obtain periodic orbits that are also localised in the spanwise direction we continue the periodic orbit in box width. For the continuation in L_z we fix a Reynolds number of $Re = 2180$. As a measure of the state we consider the energy density obtained by averaging over the downstream and normal directions,

$$E_{\parallel}(z) = \frac{1}{2L_x} \int_0^{L_x} \int_{-1}^1 \mathbf{u}^2 dx dy \quad (4.1)$$

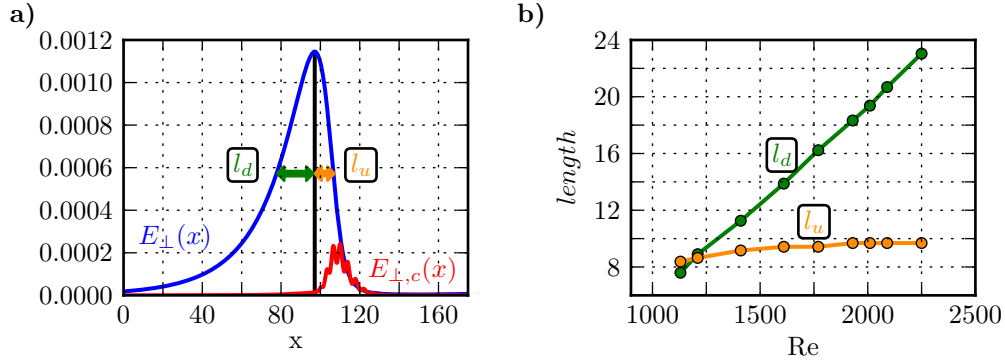


FIGURE 6. Energy profiles of the localized state. (a) Densities of total (red) and the cross flow (blue) energy for the periodic orbit at $Re = 2010$ along the flow direction, which is from left to right. The cross flow energy density is multiplied by a factor of 10. (b) Upstream l_u (orange) and downstream l_d (green) distances from the maximum to half the maximal values in energy.

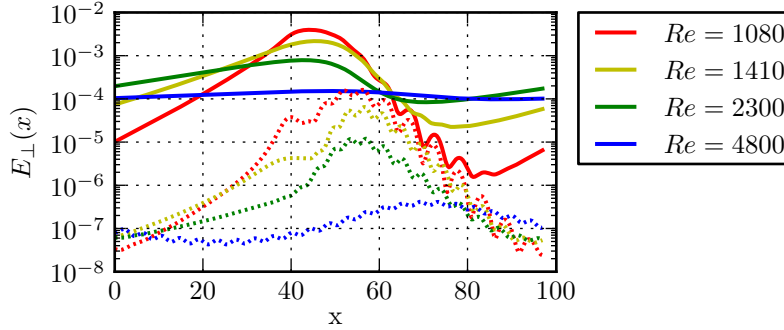


FIGURE 7. Profiles of PO_E for increasing Reynolds numbers. The solid lines show the total and the dashed lines the crossflow energy densities. Consistent with the increase in l_d , the states become more and more delocalized with increasing Reynolds number, until they merge into a spatially extended state near $Re = 5385$. The streamwise length of the computational domain is 32π .

This partially averaged energy density depends on the spanwise coordinate only, and is shown in figure 8(a) is shown for various widths L_z . The maximum at $z = 0$ corresponds to the position of the low-speed streak. For $L_z = 2\pi$ the second smaller maximum is the position of the weak high speed streak. Between 2π and 2.5π the lower maximum splits into two, and for $L_z > 5\pi$ the energy density has a very low value over most of the domain, indicating a spanwise localised flow structure. Visualisations of the periodic orbit at $Re = 2180$ in a box with $L_z = 15\pi$ using the streamwise and the spanwise velocity in the mid-plane are shown in figure 9. The logarithmic scale in figure 8(a) shows that $E_{\parallel}(z)$ does not drop off exponentially, but much more slowly. This is in marked contrast to spanwise localised, but streamwise extended states, where the energy density falls off very quickly (Gibson & Brand 2014; Melnikov *et al.* 2014).

The cross flow energy 3.2 also undergoes a qualitative change with increasing L_z , as shown in figure 8(b). As the width of the box increases, the single maximum splits into two maxima. Their location is indicated in figure 9(b), where the spanwise velocity in the midplane is shown. The figure reveals a large scale, quadrupolar-like flow field whose centres of the left and the right pairs of lobes coincide with intensity maxima of $E_{\perp,c}(x)$. It should be remarked that the quadrupole like shape of the spanwise velocity

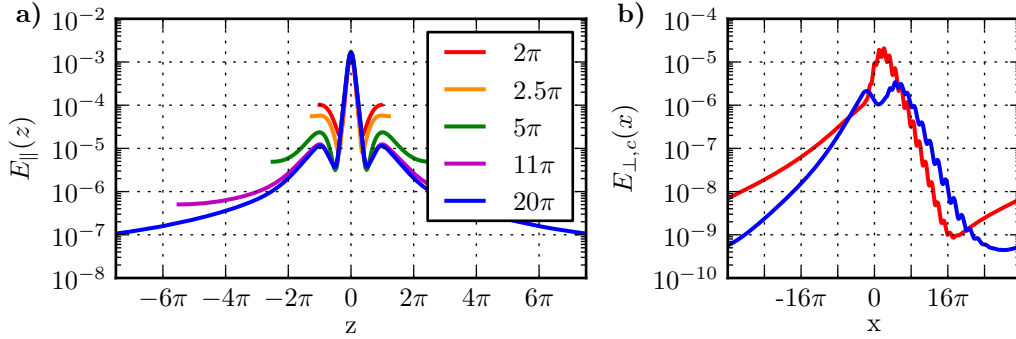


FIGURE 8. Profiles of the localized state PO_E at $Re=2180$. (a) Spanwise profiles of the total energy for various spanwise widths L_z . (b) crossflow energy densities vs. x for $L_z = 2\pi$ and 15π .

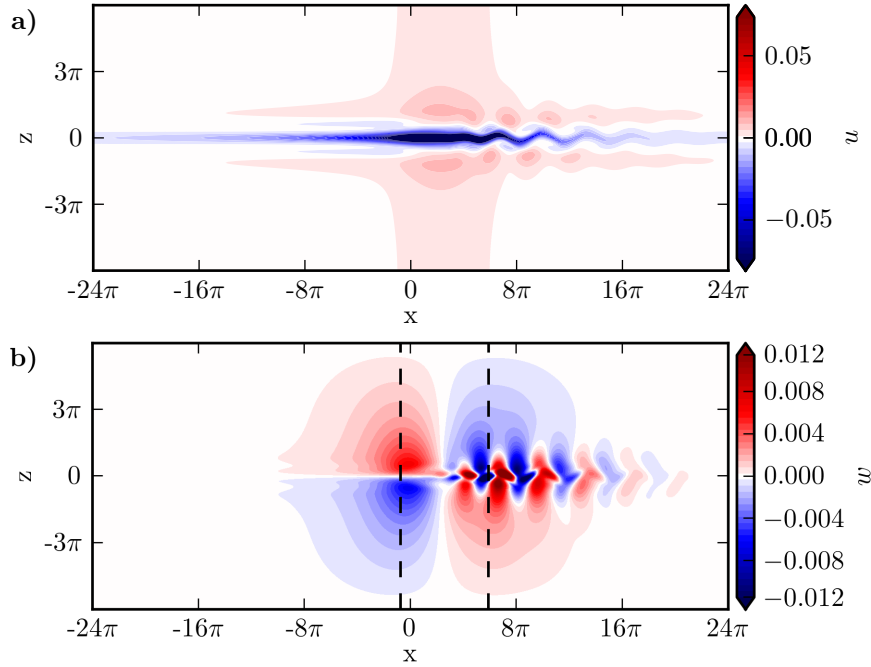


FIGURE 9. Streamwise (a) and spanwise (b) velocity in the mid-plane for the fully localised periodic orbit at $Re = 2180$. The dashed lines in (b) mark the downstream positions of the maxima in the energy density.

also exists away from the midplane, but becomes less distinct close to the walls. Given the observation of similar large scale flows in turbulent spots in plane Couette (e.g. Schumacher & Eckhardt 2001; Lagha & Manneville 2007; Duguet & Schlatter 2013) and plane Poiseuille flow (Lemoult *et al.* 2013a,b), one can anticipate that they appear for all structures that are localised in all directions.

A stability analysis of the localised state as a function of L_z at $Re = 2180$ shows that it has two unstable eigenvalues for $L_z \geq 6\pi$. Therefore, it is not an attracting state in the laminar-turbulent boundary. Edge tracking calculations starting from the disturbed localised periodic orbit do not result in a simple attractor. Instead, the time evolution of the state is chaotic, but it remains localised. This behaviour is similar to what has been

seen in large plane Couette domains (Marinc *et al.* 2010; Schneider *et al.* 2010*b*; Duguet *et al.* 2009), long pipes (Mellibovsky *et al.* 2009), or wide domains in the asymptotic suction boundary layer (Khapko *et al.* 2013*b*).

5. Conclusions and Outlook

We were able to identify a fully localised periodic orbit in plane Poiseuille flow. The orbit was shown to bifurcate from a streamwise extended travelling wave. Together with the other current examples of long-wavelength instabilities (Melnikov *et al.* 2014; Chantry *et al.* 2013) we anticipate that many more localised states can be found in bifurcations of the myriad of spatially extended states that have been identified already Gibson *et al.* (2009). Homotopies between plane Poiseuille flow and other flows, including plane Couette or the asymptotic suction boundary layer, can then reveal connections between these states (Waleffe 2003; Kreilos *et al.* 2013). More generally, the presence of localised states opens up the road to spatial delocalisation and the development of spatio-temporally patterns (see e.g. Barkley & Tuckerman 2005; Avila *et al.* 2011).

Acknowledgements We thank Yohann Duguet and Tobias Kreilos for discussions, and John Gibson for providing *channelflow*. This work was supported by the Deutsche Forschungsgemeinschaft within FOR 1182.

REFERENCES

- AVILA, K., MOXEY, D., DE LOZAR, A., AVILA, M., BARKLEY, D. & HOF, B. 2011 The onset of turbulence in pipe flow. *Science* **333** (6039), 192–196.
- AVILA, M., MELLIBOVSKY, F., ROLAND, N. & HOF, B. 2013 Streamwise-Localized Solutions at the Onset of Turbulence in Pipe Flow. *Phys. Rev. Lett.* **110**, 224502.
- BARKLEY, D. & TUCKERMAN, L. 2005 Computational Study of Turbulent Laminar Patterns in Couette Flow. *Phys. Rev. Lett.* **94**, 014502.
- CARLSON, D. R., WIDNALL, S. E. & PEETERS, M. F. 1982 A flow-visualization study of transition in plane Poiseuille flow. *J. Fluid Mech.* **121**, 487–505.
- CHANTRY, M., WILLIS, A. P. & KERSWELL, R. R. 2013 The genesis of streamwise-localized solutions from globally periodic travelling waves in pipe flow. *arXiv Prepr. arXiv1308.6224* pp. 1–5.
- DAUCHOT, O. & DAVIAUD, F. 1995 Finite amplitude perturbation and spots growth mechanism in plane Couette flow. *Phys. Fluids* **7**, 335.
- DIJKSTRA, H., *et al.* 2014 Numerical Bifurcation Methods and their Application to Fluid Dynamics: Analysis beyond Simulation. *Commun. Comput. Phys.* **15**, 1–45.
- DUGUET, Y. & SCHLATTER, P. 2013 Oblique Laminar-Turbulent Interfaces in Plane Shear Flows. *Phys. Rev. Lett.* **110**, 034502.
- DUGUET, Y., SCHLATTER, P. & HENNINGSON, D. S. 2009 Localized edge states in plane Couette flow. *Phys. Fluids* **21**, 111701.
- DUGUET, Y., SCHLATTER, P. & HENNINGSON, D. S. 2010 Formation of turbulent patterns near the onset of transition in plane Couette flow. *J. Fluid Mech.* **650**, 119–129.
- GIBSON, J. F. 2012 Channelflow: A spectral Navier-Stokes simulator in C++. *Tech. Rep.*. U. New Hampshire.
- GIBSON, J. F. & BRAND, E. 2014 Spanwise-localized solutions of planar shear flows. *J. Fluid Mech.* **745**, 25–61.
- GIBSON, J. F., HALCROW, J. & CVITANOVIĆ, P. 2009 Equilibrium and travelling-wave solutions of plane Couette flow. *J. Fluid Mech.* **638**, 243–266.
- GUENNEBAUD, G., JACON, B. & OTHERS 2010 Eigen v3.
- HEGSETH, J. 1996 Turbulent spots in plane Couette flow. *Phys. Rev. E* **54**, 4915–4923.
- HENNINGSON, D., SPALART, P. & KIM, J. 1987 Numerical simulations of turbulent spots in plane Poiseuille and boundary-layer flow. *Phys. Fluids* **30**, 2914.

- JEONG, J & HUSSAIN, F 1995 On the identification of a vortex. *J. Fluid Mech.* **285**, 69–94.
- KHAPKO, T., KREILOS, T., SCHLATTER, P., DUGUET, Y., ECKHARDT, B. & HENNINGSON, D. S. 2013a Localized edge states in the asymptotic suction boundary layer. *J. Fluid Mech.* **717**, R6.
- KHAPKO, T., DUGUET, Y., KREILOS, T., SCHLATTER, P., ECKHARDT, B. & HENNINGSON, D. S. 2013b Complexity of localised coherent structures in a boundary-layer flow. *Eur. Phys. J. E arXiv1308.5531* (in press).
- KREILOS, T. & ECKHARDT, B. 2012 Periodic orbits near onset of chaos in plane Couette flow. *Chaos* **22**, 047505.
- KREILOS, T., VEBLE, G., SCHNEIDER, T. M. & ECKHARDT, B. 2013 Edge states for the turbulence transition in the asymptotic suction boundary layer. *J. Fluid Mech.* **726**, 100–122.
- LAGHA, M. & MANNEVILLE, P. 2007 Modeling of plane Couette flow. I. Large scale flow around turbulent spots. *Phys. Fluids* **19**, 094105.
- LEMOULT, G., AIDER, J.-L. & WESFREID, J. E. 2013a Turbulent spots in a channel: large-scale flow and self-sustainability. *J. Fluid Mech.* **731**, R1.
- LEMOULT, G., GUMOWSKI, K., AIDER, J.-L. & WESFREID, J. E. 2013b Turbulent spots in channel : an experimental study Large-scale flow, inner structure and low order model. *arXiv Prepr. arXiv1311.4668* pp. 1–11.
- LUNDBLADH, A. & JOHANSSON, A. V. 1991 Direct simulation of turbulent spots in plane Couette flow. *J. Fluid Mech.* **229**.
- MARINC, D., SCHNEIDER, T. M. & ECKHARDT, B. 2010 Localized edge states for the transition to turbulence in shear flows. In *Seventh IUTAM Symp. Laminar-Turbulent Transit.* (ed. Philipp Schlatter & Dan S. Henningson), *IUTAM Bookseries*, vol. 18, pp. 253–258. Dordrecht: Springer Netherlands.
- MELLIBOVSKY, F., MESEGUER, A., SCHNEIDER, T. & ECKHARDT, B. 2009 Transition in Localized Pipe Flow Turbulence. *Phys. Rev. Lett.* **103**, 054502.
- MELNIKOV, K., KREILOS, T. & ECKHARDT, B. 2014 Long wavelength instability of coherent structures in plane Couette flow. *Phys. Rev. E* **89**, 043088.
- MOXEY, D. & BARKLEY, D. 2010 Distinct large-scale turbulent-laminar states in transitional pipe flow. *Proc. Natl. Acad. Sci. U. S. A.* **107**, 8091–8096.
- NAGATA, M. & DEGUCHI, K. 2013 Mirror-symmetric exact coherent states in plane Poiseuille flow. *J. Fluid Mech* **735**, R4.
- ORSZAG, S. A. 1971 Accurate solution of the Orr–Sommerfeld stability equation. *J. Fluid Mech.* **50**, 689–703.
- PRICE, T., BRACHET, M. & POMEAU, Y. 1993 Numerical characterization of localized solutions in plane Poiseuille flow. *Phys. Fluids A Fluid Dyn.* **5**, 762.
- SCHNEIDER, T. M., GIBSON, J. F. & BURKE, J. 2010a Snakes and Ladders: Localized Solutions of Plane Couette Flow. *Phys. Rev. Lett.* **104**, 104501.
- SCHNEIDER, T. M., GIBSON, J. F., LAGHA, M., DE LILLO, F. & ECKHARDT, B. 2008 Laminar-turbulent boundary in plane Couette flow. *Phys. Rev. E* **78**, 037301.
- SCHNEIDER, T. M., MARINC, D. & ECKHARDT, B. 2010b Localized edge states nucleate turbulence in extended plane Couette cells. *J. Fluid Mech.* **646**, 441.
- SCHUMACHER, J. & ECKHARDT, B. 2001 Evolution of turbulent spots in a parallel shear flow. *Phys. Rev. E* **63**, 046307.
- SKUFCA, J., YORKE, J. & ECKHARDT, B. 2006 Edge of Chaos in a Parallel Shear Flow. *Phys. Rev. Lett.* **96**, 174101.
- TOH, S. & ITANO, T. 2003 A periodic-like solution in channel flow. *J. Fluid Mech.* **481**, 67–76.
- VISWANATH, D. 2007 Recurrent motions within plane Couette turbulence. *J. Fluid Mech.* **580**, 339.
- WALEFFE, F. 1998 Three-Dimensional Coherent States in Plane Shear Flows. *Phys. Rev. Lett.* **81**, 4140.
- WALEFFE, F. 2003 Homotopy of exact coherent structures in plane shear flows. *Phys. Fluids* **15**, 1517.
- WANG, J., GIBSON, J. F. & WALEFFE, F. 2007 Lower Branch Coherent States in Shear Flows: Transition and Control. *Phys. Rev. Lett.* **98**, 204501.
- ZAMMERT, S. & ECKHARDT, B. 2014 Periodically bursting edge states in plane Poiseuille flow. *Fluid Dyn. Res. arXiv1312.6783* (in press) .